Geochemistry Geophysics Geosystems G3

Article
Volume 12, Number 8
11 August 2011
Q08008, doi:10.1029/2011GC003633
ISSN: 1525-2027

Published by AGU and the Geochemical Society

Combined use of magnetometry and spectroscopy for identifying magnetofossils in sediments

Jessica Kind and Andreas Ulrich Gehring
Institute of Geophysics, ETH Zurich, Sonneggstrasse 5, CH-8096 Zurich, Switzerland (jessica.kind@erdw.ethz.ch; andreas.gehring@erdw.ethz.ch)

Michael Winklhofer
Institute of Geophysics, ETH Zurich, Sonneggstrasse 5, CH-8096 Zurich, Switzerland

Department of Earth and Environmental Science, Ludwig Maximilians University, Theresienstrasse 41, D-80333 Munich, Germany (michael.winklhofer@geophysik.uni.muenchen.de)

Ann Marie Hirt
Institute of Geophysics, ETH Zurich, Sonneggstrasse 5, CH-8096 Zurich, Switzerland (ann.hirt@erdw.ethz.ch)

[1] Identification of the mineral remains of magnetotactic bacteria (MTB), known as magnetofossils, is of particular interest because their occurrence can be used for environmental and climatic reconstructions. Single-domain magnetite particles, which are biomineralized in the cell body of MTB, have characteristic properties that can be used to detect their fossil remains. Acquisition of anhysteretic and isothermal remanent magnetization (ARM and IRM), first-order reversal curve (FORC) diagrams, and ferromagnetic resonance (FMR) spectra were used to detect the magnetic mineral inventory in Holocene lake sediments. A comparative analysis in terms of the discriminatory power of these methods is presented. The FORC diagrams contain two distinct features: a sharp horizontal ridge centered on the horizontal axis B_c and a feature with symmetric spread along the vertical B_b axis. The coercivity spectra derived from the central ridge coincides with that derived from ARM and IRM acquisition curves and is compatible with the presence of noninteracting linear chains of single-domain magnetite. The second feature on FORC diagrams is indicative of interacting particles in clusters. In the FMR spectra from bulk sediment, two populations are separated empirically based on the FORC information. An asymmetric signal is taken to describe the population, which contains single-domain particles in clusters. Empirical spectral separation of this contribution results in FMR spectra that are similar to those of intact MTB, which strongly suggests that a fraction of linear magnetosome chains is present. Combination of FMR and FORC results demonstrates the strong potential of these methods for identifying magnetofossils, based on alignment and interaction patterns of magnetic particles.

Components: 7100 words, 5 figures, 1 table.

Keywords: ferromagnetic resonance spectroscopy; first-order reversal curves; magnetofossils; single-domain particles; spectral separation.

Index Terms: 1505 Geomagnetism and Paleomagnetism: Biogenic magnetic minerals; 1512 Geomagnetism and Paleomagnetism: Environmental magnetism; 1540 Geomagnetism and Paleomagnetism: Rock and mineral magnetism.

Received 23 March 2011; **Revised** 22 June 2011; **Accepted** 23 June 2011; **Published** 11 August 2011.

Kind, J., A. U. Gehring, M. Winklhofer, and A. M. Hirt (2011), Combined use of magnetometry and spectroscopy for identifying magnetofossils in sediments, *Geochem. Geophys. Geosyst.*, *12*, Q08008, doi:10.1029/2011GC003633.

1. Introduction

[2] Microorganisms are sparsely preserved in geological records. Consequently the paleoecology of microbial biota is poorly understood. In the absence of microbiological morphologies, mineral biomarkers have been taken as evidence for biological activity because of their high chemical stability under near–Earth surface conditions. Among the large group of unicellular microorganisms, magnetotactic bacteria (MTB) have the ability to produce membrane-enclosed ferrimagnetic minerals termed magnetosomes, which generally consist of magnetite (Fe_3O_4) or greigite (Fe_3S_4) [*Frankel et al.*, 1979; *Farina et al.*, 1990; *Mann et al.*, 1990; *Pósfai et al.*, 1998; *Fischer et al.*, 2011]. In most mature intact MTB, particles are aligned in a chain configuration, which creates a cellular magnetic dipole [*Frankel et al.*, 1979]. This dipole is usually large enough to interact with the Earth's magnetic field and therefore to operate as a compass to navigate MTB along field lines toward their favorable habitat [*Frankel and Blakemore*, 1980; *Kalmijn*, 1981; *Erglis et al.*, 2007]. Studies of wild-type MTB have shown that the preferred habitats for MTB is around the oxic-anoxic transition zone (OATZ) in marine environments, rivers, lakes, and soils [*Sparks et al.*, 1986; *Vali et al.*, 1987; *Bazylinski et al.*, 1988; *Fassbinder et al.*, 1990; *Simmons et al.*, 2004; *Kim et al.*, 2005; *Flies et al.*, 2005; *Moskowitz et al.*, 2008]. Until now, magnetofossils have been reported from selected deposits that may even extend in age as far back as the Precambrian, but their documentation in geological records is fragmentary [*Chang et al.*, 1989; *Stolz et al.*, 1989; *Petermann and Bleil*, 1993; *Snowball*, 1994; *Smirnov and Tarduno*, 2000; *Pan et al.*, 2005; *Housen and Moskowitz*, 2006; *Bazylinski et al.*, 2007; *Kopp and Kirschvink*, 2008; *Abrajevitch and Kodama*, 2009]. Holocene lake sediments often contain high-quality magnetosome records [e.g., *Sparks et al.*, 1986; *Vali et al.*, 1987; *Snowball*, 1994; *Oldfield et al.*, 2003; *Paasche et al.*, 2004; *Haltia-Hovi et al.*, 2010]. MTB can be used as potential biomarkers for ecological and climate reconstructions [*Snowball et al.*, 2002]. Because they are an ideal magnetic carrier of natural remanent magnetization, MTB and their fossil remains can be used to study the behavior of the Earth's magnetic field [*Løvlie and Larsen*, 1981; *Kirschvink*, 1982; *Petersen et al.*, 1986; *Snowball et al.*, 2002; *Winklhofer and Petersen*, 2007; *Kopp and Kirschvink*, 2008]. Identification of magnetofossils is more complicated because bacterial cells eventually lyse in geological systems, which results in destruction of the magnetosome chain configuration, whose mechanical stability is due to organic supporting material [*Shcherbakov et al.*, 1997; *Scheffel et al.*, 2006]. Therefore, magnetofossil preservation is vitally affected by chemical and physical conditions, such as decomposition rate of organic matter or turbulence during taphonomy [*Chang and Kirschvink*, 1989]. Depending on these conditions, MTB can be preserved as chains, chain fragments, clusters of magnetosomes or as single magnetosomes. MTB and their fossil remains are generally identified by microscopy and magnetic methods. Living MTB can be easily detected using phase contrast or differential interference contrast microscopy and a bar magnet, which dictates their movements [*Blakemore*, 1982; *Kirschvink*, 1980; *Petersen et al.*, 1986]. For detailed characterization of the morphology of magnetosomes, electron microscopy has been applied successfully [*Mann et al.*, 1987; *Bazylinski et al.*, 1994]. Microscopic methods, however, are less effective for magnetofossils that are unevenly distributed in bulk sediments. This shortcoming is often overcome by magnetic extraction [*Blakemore*, 1982]. However, if the magnetosomes are highly diluted or if they are embedded in a clay-rich and/or organic matrix, magnetic extraction has had limited success. Moreover, extraction affects the preserved configuration of magnetosomes, which is a key parameter for identification of MTB as well as magnetofossils.

[3] Magnetic methods have been used extensively to detect MTB and magnetofossils. The high sensitivity of these methods allows their application on bulk material. For improved identification of magnetofossil chains, features that can be exploited are (1) narrow grain size distribution of magnetosomes in the single-domain range and (2) pronounced shape anisotropy due to linear alignment of the magnetosomes. Both criteria can be assessed with bulk sediment samples. With the first criterion

only, ambiguity remains because such single-domain particles can also be produced by inorganic processes [*Maher and Taylor*, 1988]. In contrast, the one-dimensional assembly of magnetite particles formed without an applied magnetic field is exclusively produced by MTB [*Philipse and Maas*, 2002; *Zhang et al.*, 2009]. Intact chains generate pronounced interaction-induced shape anisotropy. Increased disintegration of chains weakens shape anisotropy. Clusters of magnetosomes and isolated magnetosomes have no detectable interaction-induced shape anisotropy. A standard magnetic approach for chain identification in bulk sediments is the test of *Moskowitz et al.* [1993]. This test uses changes in magnetic remanence properties of magnetite on warming through the Verwey transition after zero-field cooling and field cooling, respectively. The Moskowitz test leads to false conclusions if the magnetosomes are oxidized or if the magnetosome chains are mixed with a population of nonchain ferrimagnetic crystals [*Weiss et al.*, 2004; *Kopp and Kirschvink*, 2008]. Furthermore, there is still ambiguity about the robustness of this test [*Carter-Stiglitz et al.*, 2002, 2003; *Weiss et al.*, 2004; *Fischer et al.*, 2008].

[4] In recent years, different rock magnetic parameters, mainly inferred from hysteresis properties or remanence measurements, have been used to detect MTB [*Lascu et al.*, 2010]. Among the different methods, first-order reversal curves (FORCs) have been a valuable tool because they are sensitive to interactions [*Pike et al.*, 1999] and variations in domain state [*Roberts et al.*, 2000]. Moreover, detailed analysis of FORC diagrams of sediments that are known to contain abundant magnetofossils contain characteristic features that have been interpreted as evidence for chain configurations [*Chen et al.*, 2007; *Abrajevitch and Kodama*, 2009; *Paasche and Larsen*, 2010; *Egli et al.*, 2010]. This interpretation is based on the assumption that magnetosomes with interaction-induced shape anisotropy [*Penninga et al.*, 1995; *Hanzlik et al.*, 2002; *Muxworthy and Williams*, 2006] act as noninteracting or weakly interacting uniaxial single-domain particles [*Egli et al.*, 2010].

[5] A powerful method for detecting anisotropy effects is ferromagnetic resonance (FMR) spectroscopy [*Bickford*, 1950; *Vonsovskii*, 1966]. Studies of intact MTB reveal characteristic spectral features, which are caused by the difference in magnetization parallel and perpendicular to the axes of one-dimensional assemblies of magnetosomes [*Weiss et al.*, 2004; *Kopp et al.*, 2006; *Kopp and Kirschvink*, 2008; *Fischer et al.*, 2008]. The few FMR studies that have been performed on magnetofossils reveal less pronounced spectral traits [*Kopp and Kirschvink*, 2008]. This is due to the fact that in geological samples magnetofossils are preserved in different configurations. Despite the fact that the different magnetic methods provide specific information about the occurrence of magnetofossils, their unambiguous detection is still critical.

[6] The purpose of this study is to investigate whether FORC and FMR data reflect the same magnetic characteristics, and whether they can be mutually supportive in interpreting the presence of magnetofossil chains. The robustness of this combined approach for improved identification of magnetofossils is discussed using Holocene lake sediments as an example.

2. Samples and Methods

2.1. Sediment Samples

[7] The sediments were obtained from the Soppensee, a closed limnological system with negligible detrital input, that was formed during the last glaciation in central Switzerland [*Lotter*, 2001]. Samples were collected from a dark gray layer of about one meter thickness within a ≈8 m long piston core. Sedimentological and geochemical analyses indicate that this layer is characterized by organic carbon contents of about 20% and a sulfur content below the detection limit [*Fischer*, 1996], which indicates predominantly postoxic conditions [*Berner*, 1981; *Lotter*, 2001]. This mid-Holocene layer is indicative of a paleo-OATZ, and is therefore a likely host for magnetofossils. Considering the low sulfur content in this environment, magnetofossils are most likely magnetite and/or maghemite. Along a profile through this layer, 66 samples were collected in 12 cm^3 cubes. Five samples (236, 237, 239, 243, and 245) were taken within the dark grey, organic-rich layer for detailed assessment of magnetic properties.

2.2. Magnetic Measurements

2.2.1. Remanent Magnetization

[8] Acquisition and demagnetization of an isothermal remanent magnetization (IRM) were performed on each cube to determine remanence coercivity spectra. The IRM was acquired in fields up to 1.5 T using an ASC Scientific Pulse Magnetizer model IM-10-30. IRM measurements were repeated twice for both the acquisition and

demagnetization curves. IRM acquisition and its demagnetization were performed in 20 and 40 steps, respectively. An anhysteretic remanent magnetization (ARM) was imparted along the z axis of the cube in a 120 mT alternating field (AF) with a DC bias field of 0.1 mT after the sample had been demagnetized along three orthogonal axes with a maximum peak field of 150 mT. AF demagnetization was performed with up to 80 steps of increasing peak field intensity along the direction of the ARM. To increase experimental precision, the ARM procedure was repeated 7 times for sample 237 and 3 times for the other samples. IRM and ARM were measured with a 2G Enterprises, model 755R, three-axis DC-SQUID rock magnetometer and were normalized using the maximum magnetization to obtain the median destructive field (MDF). The MDF is defined as the AF demagnetization field needed to reduce the initial saturated remanence by one half.

2.2.2. Induced Magnetization

[9] Low-field magnetic susceptibility was measured using an AGICO KLY-2 Kappabridge magnetic susceptibility meter. Hysteresis properties were measured in sweeping mode using a Princeton Measurements Corporation MicroMag 2900 alternating gradient magnetometer (AGM) in fields up to 1 T with an averaging time of 100 ms. Saturation magnetization (M_s), saturation remanence (M_{rs}) and coercivity (B_c) were determined after correction for linear contribution of the paramagnetic and diamagnetic phases. The remanent magnetization imparted at 1 T was then demagnetized in a backfield to obtain the coercivity of remanence (B_{cr}). Measurements for sample 237 were made on 4 subsamples of about 4 mg each. A single measurement was made on a subsample of the remaining samples (236, 239, 243, and 245).

[10] First-order reversal curves (FORCs) were measured to obtain a detailed analysis of the B_c spectrum of the five samples and to estimate magnetic interactions [*Pike et al.*, 1999; *Roberts et al.*, 2000]. These partial hysteresis curves were measured on the AGM by saturating the sample at 1 T, decreasing the field down to a determined value, and reversing the field sweep again to the saturation state. The procedure was repeated in a series of steps following the protocol described by *Roberts et al.* [2000]. The intrinsic parameters that are responsible for the span and resolution of the FORC diagram were set at ±80 mT for the vertical axis, and between 0 and 100 mT for the horizontal axis. The field increment ΔB was different for each samples. The highest resolution, with $\Delta B = 0.5$ mT, resulted in measurement of 541 FORCs for sample 237. The other four samples were measured with ΔB of around 2 mT and therefore with fewer FORCs.

[11] The intrinsic resolution of each FORC data set is high enough to clearly identify a central ridge for the chosen field increment [*Egli et al.*, 2010]. The central ridge is characterized by a broad horizontal and a narrow vertical distribution in the FORC diagram. Vertical spreads around $B_b = 0$ are expressed as $B_{b,1/2}$. FORC diagrams were calculated using a MATLAB code [*Winklhofer and Zimanyi*, 2006] and subtraction of the central ridge was done as described by *Egli et al.* [2010]. To isolate the central ridge from the FORC diagram, a narrow horizontal strip containing the ridge was extracted and the remaining FORC distribution was interpolated across the strip. To verify the robustness of the approach, horizontal strips of different width were extracted from the FORC distribution, which resulted in approximately the same central ridge function. To represent the FORC diagrams that contain the central ridge and the ridge-free FORC function, a value of $SF = 3$ was used [*Roberts et al.*, 2000], which removes most of the measurement noise and avoids excessive broadening of the FORC function. In addition, the calculated parameter I_{CR}, which is the integral of the central ridge, was determined to estimate the contribution of the different magnetic populations to M_{rs} [*Egli et al.*, 2010].

2.2.3. Electron Magnetic Spectroscopy

[12] Electron magnetic resonance analysis can be subdivided schematically into electron paramagnetic resonance (EPR) and ferromagnetic resonance (FMR) spectroscopy. For paramagnetic species, such as molecules, ions or atoms possessing electrons with unpaired spins, the absorption of microwave energy is measured as a function of the applied field B. Absorption occurs when the resonance condition

$$\hbar \cdot \nu = g \cdot \mu_B \cdot \mathrm{B} \quad (1)$$

is fulfilled, where $\hbar$ is Planck's constant ($6.626 \cdot 10^{34}$ Js), ν is the microwave frequency, g is the splitting factor, μ_B the Bohr magneton ($9.274 \cdot 10^{-24}$ J/T), and B the applied magnetic field. In contrast to EPR, FMR spectroscopy detects coupled spins of a magnetically ordered phase. In this case, the applied field that established resonance conditions is affected by the internal field (B_{int})

Table 1. Summary of Magnetic Parameters

Sample	B_c [a](mT)	B_{cr} [a](mT)	M_{rs} [a]($Am^2\ kg^{-1}$)	M_s [a]($Am^2\ kg^{-1}$)	M_{rs}/M_s [a]	B_{cr}/B_c [a]	I_{CR}/M_{rs} [b]
236	22.5	35.5	$6.05\ 10^{-02}$	$1.71\ 10^{-01}$	0.36	1.57	0.21
237	22.7	34.7	$7.52\ 10^{-02}$	$1.92\ 10^{-01}$	0.39	1.52	0.24
239	23.1	34.1	$9.31\ 10^{-02}$	$9.31\ 10^{-03}$	0.41	1.47	0.24
243	23.9	35.2	$1.03\ 10^{-01}$	$2.61\ 10^{-01}$	0.39	1.47	0.21
245	24.6	35.8	$1.13\ 10^{-01}$	$1.13\ 10^{-01}$	0.41	1.45	0.25

[a]Hysteresis parameter.
[b]FORC parameter.

generated in the sample. Therefore, the resonance field (B_{res}) is the sum of the applied field B and the internal fields B_{int}. The latter is the sum of all anisotropy fields (e.g., magnetocrystalline and shape) in the magnetic material, which cannot be measured directly. In FMR spectroscopy the equation

$$\hbar \cdot \nu = g_{eff} \cdot \mu_B \cdot B_{res} \quad (2)$$

is often used, where B_{res} is the resonance field, obtained from the applied field at maximum absorption, and g_{eff} is the corresponding effective g factor. Considering equation (2), the measured g_{eff} value takes into account the influence of B_{int}. The line width ΔB and the asymmetry ratio A are two additional parameters used to describe the FMR spectra [*Weiss et al.*, 2004; *Kopp et al.*, 2006]. ΔB is defined as the full width at half maximum of the absorption spectrum. The subdivision of ΔB into ΔB_{low} and ΔB_{high} with respect to B_{res} is used to determine the asymmetry ratio $A = \Delta B_{high}/\Delta B_{low}$, where $\Delta B_{high} = B_{high} - B_{res}$, $\Delta B_{low} = B_{res} - B_{low}$, and B_{high} and B_{low} are the maximum and minimum fields of the half maximum absorption from the FMR spectrum, respectively.

[13] FMR measurements were made on sample 237, which was also used for the high-resolution FORC analysis. The spectra were acquired using an X band Bruker EMX spectrometer. For room temperature measurements, the microwave power was set at 2 mW, with modulation amplitude of 0.1 mT, microwave frequency of 9.87 GHz, and the spectra were integrated over three sweeps of the applied field from 0 to 600 mT. For the measurements at 100 K the same settings were used, except the adjusted microwave frequency was slightly lower (9.41 GHz).

[14] If room temperature and low-temperature FMR spectra are similar, it can be assumed that the magnetic particles do not undergo a Verwey transition, which erases the pronounced shape anisotropy. The absence of such a transition in natural samples can be explained by partial oxidation or maghemitization of magnetite [*Kakol and Honig*, 1989; *Özdemir et al.*, 1993]. This oxidation, however, could either be the effect of a diagenetic process or a result of storage under ambient conditions.

[15] The FMR spectrum represents a superposition of responses due to all magnetic particles in a sample, therefore an empirical spectral separation approach is used to isolate different magnetic configurations [*Gehring et al.*, 2011]. This approach takes advantage of the fact that the spectral parameters A and g_{eff} of single particles and clusters are different to those assembled in chains [*Vastyn et al.*, 1962; *Weiss et al.*, 2004; *Mastrogiacomo et al.*, 2010].

3. Results

3.1. Magnetization and Demagnetization Properties

[16] Magnetic susceptibility measurements of the 66 samples along the profile of the dark gray layer have a mean value of $(2.00 \pm 0.33) \cdot 10^{-6}$ m^3/kg. The low standard deviation suggests small variations in magnetic mineral concentration. The five samples selected from the profile have similar hysteresis parameters (Table 1). B_c is 23.4 ± 0.96 mT and B_{cr} = 34.7 ± 1.08 mT, which leads to a B_{cr}/B_c ratio of 1.49 ± 0.05, and a M_{rs}/M_s ratio of 0.40 ± 0.05. Therefore, the samples selected for detailed magnetic analysis can be considered representative.

[17] Detailed analyses on the four subsamples from sample 237 gives hysteresis values of B_c = 22.4 ± 0.2 mT, B_{cr} = 33.7 ± 0.6 mT, M_{rs} = 7.4 ± 1.7 10^{-2} Am^2/kg and $M_s = 1.89 \pm 4.1\ 10^{-1}$ Am^2/kg. The remanence ratio M_{rs}/M_s = 0.41 ± 0.01 and the coercivity ratio $B_{cr}/B_c = 1.50 \pm 0.02$ indicate that the ferrimagnetic particles are in a single-domain state (Figure 1).

[18] ARM and IRM demagnetization results for sample 237 (Figure 2) are characteristic of single-domain magnetite particles [*Moskowitz et al.*, 1988]. The MDF of the normalized ARM acquisition and demagnetization curves is about 45 mT.

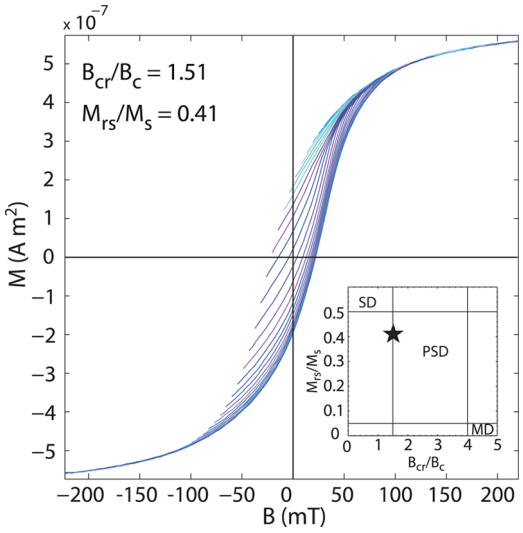

Figure 1. Set of FORCs for the studied Soppensee sample 237. Every second FORC measurement, after subtraction of the paramagnetic mineral contribution, is shown for clarity. The inset on the right-hand side is a Day plot [*Day et al.*, 1977] with data for this sample, which fall close to the expected field for single-domain particles.

The median acquisition, and accordingly, median destructive field of the IRM is about 40 mT. In both cases, $MDF_{ARM} > MDF_{IRM}$, with MDF_{ARM}/MDF_{IRM} = 1.21 and 1.09 for the acquisition and demagnetization curves, respectively. Results of the modified Lowrie-Fuller test are of L type [cf. *Johnson et al.*, 1975], which are considered to be characteristic of single-domain particles [*Lowrie and Fuller*, 1971; *Johnson et al.*, 1975; *Xu and Dunlop*, 1995]. Furthermore, the crossover point of the IRM curves at 0.48 reflects the symmetry of the acquisition and demagnetization behavior [*Cisowski*, 1981], which indicates noninteracting single-domain grains.

[19] To analyze the maximum loss and maximum gain in magnetization, the derivative of the curves (Figure 2) was calculated and plotted on a log scale between 10 and 120 mT. Differences between the IRM and ARM curves can be seen by the lateral shift of the maxima in the derivative of the coercivity distributions with slightly lower IRM values than ARM (Figures 2b and 2c). This slight shift can be explained because IRM takes into account all particles, whereas ARM selectively responds to noninteracting particles with coercivity below the maximum AF applied field during ARM acquisition [e.g., *Egli and Lowrie*, 2002; *Kobayashi et al.*, 2006]. The IRM and ARM acquisition curves were decomposed into magnetic coercivity components, assuming that acquisition curves are a linear addition of different Gaussian components. Both IRM and ARM component analysis indicates two dominant components, with a low-coercivity and a high-coercivity component. The relative abundance of these two components was varied by trial and error so as to achieve a best fit. In Figure 2b, the IRM decomposition analysis enables identification of a mean coercivity of around 37 mT for the low coercivity component and a mean coercivity of around 59 mT for the high-coercivity component. ARM decomposition results in mean coercivities of around 40 mT and 64 mT for the low- and high-coercivity components, respectively. The two coercivity components agree well with the "biogenic

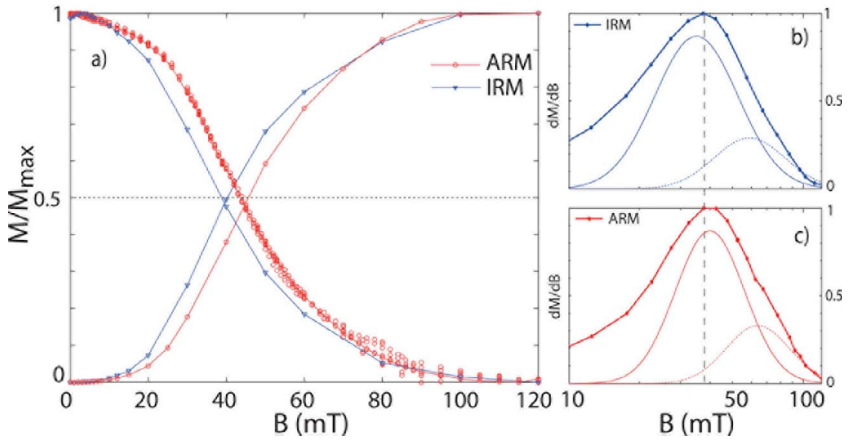

Figure 2. Detailed ARM and IRM acquisition and demagnetization curves for sample 237. (a) The intersection point of the acquisition and demagnetization curves indicates negligible interactions [*Cisowski*, 1981]. (b, c) The maximum loss, and accordingly maximum gain, is shown by the first derivative of the ARM and IRM curves. Decomposition of the remanence curves result in a low-coercivity (solid line) component and a high-coercivity (dotted line) component.

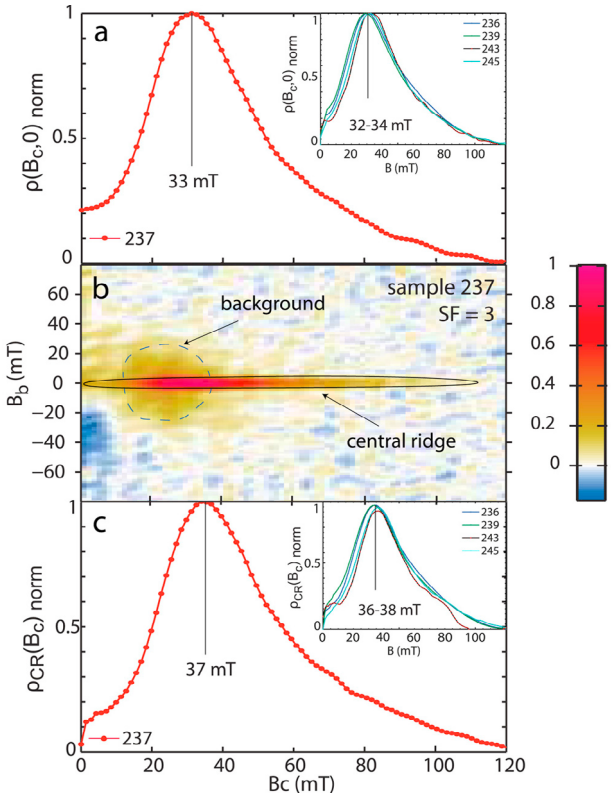

Figure 3. Analysis of first-order reversal curves for the five studied samples. (a) A partial coercivity distribution from the entire FORC distribution (background signal and central ridge) taken along $B_b = 0$ with a maximum peak field of 33 mT for sample 237. The remaining samples have similar maximum peak coercivities between 32 and 34 mT (inset). (b) A typical FORC diagram with the central ridge indicated with a black contour line and the background signal indicated by the dashed blue contour lines. (c) The coercivity distribution from the isolated central ridge has a maximum peak field of 37 mT for sample 237. The remaining samples result in maximum peak coercivities between 36 and 38 mT (inset). Each spectrum was normalized by its maximum B_c value.

soft" and "biogenic hard" components, which *Egli* [2004] consistently identified in various sediments.

3.2. FORC Analysis

[20] The five sediment samples (236, 237, 239, 243 and 245) have similar FORC diagrams to that of sample 237 (Figure 3). The principal feature is a broad B_c distribution in a range between 10 and 100 mT with a maximum at B_c = 37 mT and $B_{b,1/2}$ around 0 mT (Figure 3). This central ridge is characteristic of uniaxial noninteracting single-domain switching units, e.g., interacting particles aligned in chains [*Egli et al.*, 2010]. The small vertical spread of the central ridge is due to the discrete nature of the measurement protocol and the convolution imposed by taking a numerical mixed derivative over $(2SF + 1)^2$ grid points for each (B_b, B_c) [*Egli et al.*, 2010]. The full width at half maximum converges to the field spacing *dB* when SF goes to zero. This suggests that the central ridge in these sediments is due to noninteracting uniaxial switching units. I_{CR} is close to $M_{rs}/4$ (Table 1), which indicates that roughly half of the total saturation remanence is carried by uniaxial noninteracting single-domain switching units. After separation of the central ridge from the FORC diagram, a second feature becomes more apparent (Figure 3b, dotted line), which is centered at $B_c \approx 25$ mT and spreads in the $\pm B_b$ direction with a full width at half maximum of about 20 mT. This vertical spread is indicative of interacting particles [*Pike et al.*, 1999; *Roberts et al.*, 2000; *Egli*, 2006]. A comparison of the horizontal profile through the entire FORC distribution, $\rho(B_c, 0)/\rho(33\text{ mT}, 0)$, and the simple switching-field distribution of the central ridge, $\rho_{cr}(B_c)/\rho_{cr}(37\text{ mT})$, indicates a slight shift of the latter to higher B_c. The maximum coercivity of the entire FORC distribution peaks at 33 mT (Figure 3a), while the maximum coercivity of the simple central ridge function peaks at 37 mT for sample 237 (Figure 3c). This shift, which is seen for all studied samples, is similar to the

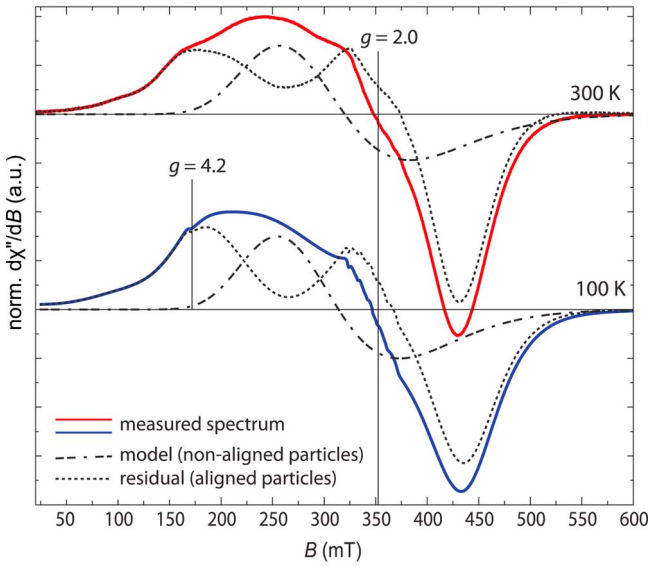

Figure 4. FMR signal obtained at 300 K (red) and 100 K (blue) for sample 237. The spectrum for nonaligned particles was modeled using the derivative of a lognormal distribution of particle volumes. After subtraction of the lognormal distribution from the measured spectrum, the residual is characteristic of linear aligned particles as expected for intact magnetofossil chains.

one observed in the comparison between ARM and IRM (Figure 2).

[21] There is little variation among the five samples in terms of their $\rho(B_c, 0)$ profiles, which all have roughly a lognormal shape with a mean peak value of 33.5 ± 1.2 mT (Figure 3a, inset). The same holds for the central ridge, which has a mean peak field of 37.4 ± 1.4 mT (Figure 3c, inset). The slightly lower maximum peak fields obtained from the isolated ridges can be explained by larger *dB* values. The other four samples also have a more diffuse FORC distribution that remains after isolation of the central ridge, which is similar to what is found in sample 237. To summarize, the FORC diagrams consistently reveal two distinct magnetic populations, which can be distinguished by their interaction and coercivity properties.

3.3. Spectroscopic Data

[22] The FMR spectrum for sample 237 at room temperature (Figure 4) is broad with no zero-field absorption. This implies the absence of magnetically soft multidomain particles, whose domain walls readily absorb microwave energy [*Polder and Smit*, 1953; *Gehring et al.*, 2009]. The low-field absorption of the FMR spectrum occurs at about 125 mT, peaks at 242 mT, and has two shoulders at 166 mT and 324 mT, respectively. The spectral parameters are B_{res} = 348 mT, which corresponds to g_{eff} = 2.03. The line width ΔB is 199 mT, and consists of ΔB_{low} = 85 mT and ΔB_{high} = 114 mT for the low field and high field absorption, respectively. The calculated asymmetry ratio A is 0.72.

[23] The FMR spectrum at 100 K has small differences compared to the spectrum measured at 300 K. The B_{res} of 347 mT corresponds to g_{eff} = 2.04, ΔB = 212 mT, and A = 0.67. In addition, two relatively weak features at g = 4.2 and g = 2 are found at low temperature (Figure 4). The fact that these features occur upon cooling is indicative of paramagnetic species in trace concentrations and they can be assigned to Fe(III) and Mn(II) [e.g., *Hall et al.*, 1974; *Granwehr et al.*, 2004]. The paramagnetic signals will not be discussed further.

[24] Considering that magnetite can occur in different geometrical configurations, all of which contribute to the FMR absorption, a spectral separation is applied. For simplification, two configurations are assumed to occur in the natural bulk material. One contains magnetite particles that are aligned in linear chains, and the other consists of magnetite and/or maghemite particles that occur in other than one-dimensional arrangement. The spectral responses of the two configurations are distinguishable by means of g_{eff} and A values [*Vastyn et al.*, 1962; *Kopp et al.*, 2006; *Fischer et al.*,

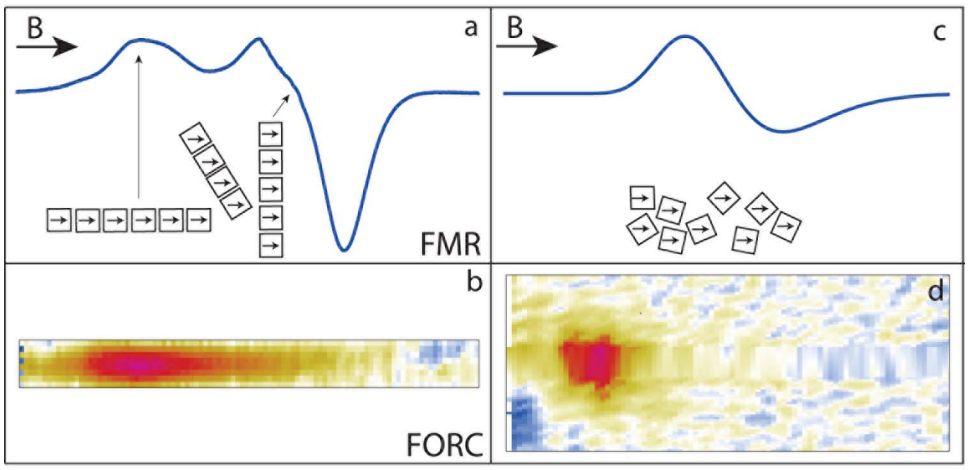

Figure 5. Schematic comparison of the diagnostic capability of FORC and FMR for identifying the presence of magnetofossils in sediments. (a) Typical FMR spectra for linear magnetite chain assemblies are related to (b) the central ridge of the FORC function. (c) The FMR signal for aggregates of magnetofossils with a lognormal distribution of particle volumes is related to the continuous background signal remaining after subtraction of the central ridge in the FORC diagram. (d) Here the upper domain ($B_b > 0$) contains the pure background signal, whereas the lower domain ($B_b < 0$) contains the pure background signal plus contributions from reversible processes related to interacting single-domain switching units as, for example, the coherent blue (negative) region in the lower left [cf. *Newell*, 2005].

2008]. For nonaligned particles, the derivative of a lognormal spectrum for particle volume was taken with $g_{eff} = 2.2$, $A \approx 1.1$, $\Delta B \approx 120$ mT and a signal intensity adjusted to the measured spectrum [*Vastyn et al.*, 1962; *Gehring et al.*, 2011]. Subtraction of this contribution yields the second population with $g_{eff} = 1.88$ and $A \approx 0.4$. To our knowledge values of $g_{eff} < 2$ for single-domain magnetite has been reported only for intact magnetosome chains [*Weiss et al.*, 2004; *Kopp et al.*, 2006]. The FMR signals at 100 K and at room temperature is similar, therefore the parameterization for nonaligned particles was adopted with $B_{res} = 300$ mT and a corresponding $g_{eff} = 2.3$. The remaining signal has $g_{eff} = 1.91$ and $A \approx 0.5$.

4. Discussion

[25] All magnetic measurements clearly indicate that the sediment samples are magnetically dominated by magnetite particles in a stable single-domain state. The occurrence of such a narrow distribution of particle size in a closed limnological system, such as Soppensee, suggests biologically-controlled magnetite formation. FORC diagrams contain evidence of two magnetic populations, which differ in their B_c distribution and in their interaction field distribution. The population forming the central ridge with $B_{b,1/2}$ around zero represents magnetically isolated switching units. These units can be well-dispersed individual particles or one-dimensional assemblies of particles, such as linear chains of magnetosomes. In the latter case, the particles have a strong dipolar coupling along the chain axis and undergo magnetization switching at a single switching field. In order for linear magnetosome chains to contribute to the central ridge, they must be well dispersed in the sediment. Otherwise, magnetic interactions with chains nearby will introduce a bias toward lower or higher switching fields. Compared to nonaligned particles, chain configurations generally have enhanced B_c due to the interaction-induced uniaxial anisotropy [*Jacobs and Bean*, 1955; *Penninga et al.*, 1995; *Hanzlik et al.*, 2002]. The second population, whose magnetic contribution is approximately the same as for the noninteracting population according to I_{CR}, is characterized by a continuous distribution of interaction fields, which indicates aggregations of chains or to clusters of particles with isotropic interactions. It has been shown that clustering increases $B_{b,1/2}$ and reduce B_c for a given intrinsic microcoercivity [*Wohlfarth*, 1958; *Pike et al.*, 1999; *Egli*, 2006]. As seen in Figure 3b, the second population has a vertical spread of about 10 mT and a maximum B_c that is about 10 mT lower than the maximum B_c of the central ridge (Figure 3c). We surmise that both magnetic populations have roughly similar distributions of intrinsic microcoercivities, or, in other words, both populations consist of similar

particles, but reflect two distinctly different geometric arrangements or degrees of dispersion. Given the biologically-controlled origin of the magnetite in these lake sediments, it is likely that this magnetically interacting component represents collapsed magnetosome chains (Figures 5b and 5d). *Kobayashi et al.* [2006] also showed that coercivity is reduced as linear chain structure is disrupted.

[26] The Wohlfarth-Cisowski test with an R_{IRM} value of 0.48 suggests that interactions in the sample are negligible altogether [*Wohlfarth*, 1958; *Cisowski*, 1981], although a population of particles with interactions is evident in the FORC diagrams. This discrepancy may arise because B_c in the FORC measurements is more sensitive to interacting single-domain grains than the MDF_{IRM} used in the Wohlfarth-Cisowski test, which is a nonlinear parameter of the interaction strength.

[27] FMR can be used to distinguish magnetite particle configurations based on their anisotropy properties. It is well known that intact MTB have two characteristic FMR absorption peaks, a low-field peak, which is due to chains that are oriented parallel to the external field, and a peak at $g \approx 2$, which is due to chains that are oriented perpendicular to the external field [*Kopp et al.*, 2006; *Charilaou et al.*, 2011]. A similar pattern is obtained by subtracting the derivative of a lognormal curve from the measured spectrum (Figure 4). It can be postulated that the residual FMR signal, which consists of two low-field absorption peaks (Figure 5a) and the central ridge in the FORC diagram (Figure 5b) both originate from the same particle population, i.e., from intact magnetosome chains. On the other hand, the lognormal curve in the FMR analysis represents nonaligned particles clustered in the sediment matrix (Figure 5c). In contrast to aligned particles, clustered particles are characterized in the FORC diagram by a relatively narrow B_c distribution and relatively higher $B_{b,1/2}$ (Figure 5d). We interpret the clustered particles in these sediments as collapsed magnetosome chains.

[28] Theoretically, it is also possible to produce the coercivity distributions of the noninteracting uniaxial component with well-dispersed (noninteracting) elongated magnetite or maghemite particles with relatively narrow distributions of axial ratios (e.g., 1.3 to 1.8). No natural inorganic process is known, however, to produce particle chains with a narrow distribution of grain size and grain shape, and with consistent crystallographic orientation along the chain axis. The characteristic [111] alignment within magnetite-magnetosome chains [*Mann et al.*, 1987; *Buseck et al.*, 2001; *Lins et al.*, 2005; *Abracado et al.*, 2010] is required to produce the observed FMR spectra [*Charilaou et al.*, 2011]. This strongly supports the interpretation that the magnetic particle population that gives rise to the central ridge in the FORC diagram arises from magnetosomes in a linear configuration. While most species of MTB construct chains with one string of magnetosomes, there are species that construct double or multiple chain structures, in which magnetic switching does not happen in a single step [*Penninga et al.*, 1995; *Hanzlik et al.*, 2002]. How these complicated switching processes manifest themselves in FORC diagrams remains to be studied. Even though the combined FORC and FMR method enables identification of magnetosome chains, it is not possible to differentiate whether the chains consist of one string or of multiple strings.

5. Conclusions

[29] The essential requirement for unambiguous detection of magnetofossils is the preservation of magnetosomes in chains. Preservation of such assemblies in the geological record is critically affected by the decay of cellular matter, which can lead to chain collapse. In natural systems, magnetite particles occur generally in different geometrical configurations, which can obscure the signature of chain assemblies. As we have shown, this problem can be overcome by employing both FORC and FMR methods in combination. These techniques complement each other by capitalizing on their ability to distinguish coercivity and anisotropy effects, respectively. Application of these methods in connection to Holocene lake sediments demonstrates that FORC diagrams are capable of distinguishing different magnetite configurations with distinct bias field resolved coercivity spectra, i.e., interacting (clusters of magnetic particles) and noninteracting switching units (e.g., chains). FMR spectroscopy differentiates anisotropy properties, i.e., aligned and nonaligned particle configurations. Combining the two kinds of information permits assignment of physical properties to chain configurations, which is compatible with MTB and their fossil remains. The proposed combined approach is an avenue for more advanced detection of magnetofossils and their distribution in natural materials in the geological record.

Acknowledgments

[30] We thank William Lowrie for critical discussion of the manuscript and Inés Garcia Rubio for her assistance in recording the FMR spectra. We also thank Andrew P. Roberts for his input to improve the manuscript and two anonymous reviewers for their constructive reviews. The research was financially supported by the CHIRP1 project of ETH (CH1-02-08-2). M. Winklhofer acknowledges an ETH Guest Professorship, funded by ETH Fonds 0-06002-91.

References

Abracado, L. G., F. Abreu, C. N. Keim, A. P. C. Campos, U. Lins, and M. Farina (2010), Magnetosome chain superstructure in uncultured magnetotactic bacteria, *Phys. Biol.*, *7*, 11–22.

Abrajevitch, A., and K. Kodama (2009), Biochemical vs. detrital mechanism of remanence acquisition in marine carbonates: A lesson from K-T boundary interval, *Earth Planet. Sci. Lett.*, *286*, 269–277.

Bazylinski, D. A., R. B. Frankel, and H. W. Jannasch (1988), Anaerobic magnetite production by a marine, magnetotactic bacterium, *Nature*, *334*, 518–519.

Bazylinski, D. A., A. J. Garratt-Reed, and R. B. Frankel (1994), Electron microscopic studies of magnetosomes in magnetotactic bacteria, *Microsc. Res. Tech.*, *27*, 389–401.

Bazylinski, D. A., R. B. Frankel, and K. O. Konhauser (2007), Modes of biomineralization of magnetite by microbes, *Geomicrobiol. J.*, *24*, 465–475.

Berner, R. A. (1981), A new geochemical classification of sedimentary environments, *J. Sediment. Petrol.*, *51*, 359–365.

Bickford, L. R. (1950), Ferromagnetic absorption in magnetite single crystals, *Phys. Rev.*, *78*, 449–457.

Blakemore, R. P. (1982), Magnetotactic bacteria, *Annu. Rev. Microbiol.*, *36*, 217–223.

Buseck, P. R., R. E. Dunin-Borkowski, B. Devouard, R. Frankel, M. R. McCartney, P. A. Midgley, M. Pósfai, and M. Weyland (2001), Magnetite morphology and life on Mars, *Proc. Natl. Acad. Sci. U. S. A.*, *98*, 13,490–13,495.

Carter-Stiglitz, B., B. Moskowitz, and M. Jackson (2002), Low-temperature remanence in stable single domain magnetite, *Geophys. Res. Lett.*, *29*(7), 1129, doi:10.1029/2001GL014197.

Carter-Stiglitz, B., B. Moskowitz, and M. Jackson (2003), Correction to "Low-temperature remanence in stable single-domain magnetite", *Geophys. Res. Lett.*, *30*(21), 2113, doi:10.1029/2003GL018727.

Chang, S.-B. R., and J. L. Kirschvink (1989), Magnetofossils, the magnetization of sediments, and the evolution of magnetite biomineralization, *Annu. Rev. Earth Planet. Sci.*, *17*, 169–195.

Chang, S.-B. R., J. F. Stolz, J. L. Kirschvink, and S. M. Awramik (1989), Biogenic magnetite in stromatolites. II. Occurrence in ancient sedimentary environments, *Precambrian Res.*, *43*, 305–315, doi:10.1016/0301-9268(89)90061-2.

Charilaou, M., M. Winklhofer, and A. U. Gehring (2011), Simulation of ferromagnetic resonance spectra of linear chains of magnetite nanocrystals, *J. Appl. Phys.*, *109*, 093903, doi:10.1063/1.3581103.

Chen, A. P., R. Egli, and B. M. Moskowitz (2007), First-order reversal curve (FORC) diagrams of natural and cultured biogenic magnetic particles, *J. Geophys. Res.*, *112*, B08S90, doi:10.1029/2006JB004575.

Cisowski, S. (1981), Interacting vs. non-interacting single-domain behavior in natural and synthetic samples, *Phys. Earth Planet. Inter.*, *26*, 56–62.

Day, R., M. Fuller, and V. A. Schmidt (1977), Hysteresis properties of titanomagnetites: Grain-size and compositional dependence, *Phys. Earth Planet. Inter.*, *13*, 260–267.

Egli, R. (2004), Characterization of individual rock magnetic components by analysis of remanence curves. 3. Bacterial magnetite and natural processes in lakes, *Phys. Chem. Earth*, *29*, 869–884.

Egli, R. (2006), Theoretical aspects of dipolar interactions and their appearance in first-order reversal curves of thermally activated single-domain particles, *J. Geophys. Res.*, *111*, B12S17, doi:10.1029/2006JB004567.

Egli, R., and W. Lowrie (2002), Anhysteretic remanent magnetization of fine magnetic particles, *J. Geophys. Res.*, *107*(B10), 2209, doi:10.1029/2001JB000671.

Egli, R., A. Chen, M. Winklhofer, K. P. Kodama, and C.-S. Horng (2010), Detection of non-interacting single-domain particles using first-order reversal curve (FORC) diagrams, *Geochem. Geophys. Geosyst.*, *11*, Q01Z11, doi:10.1029/2009GC002916.

Erglis, K., Q. Wen, V. Ose, A. Zeltins, A. Sharipo, P. A. Janmey, and A. Cebers (2007), Dynamics of magnetotactic bacteria in a rotating magnetic field, *Biophys. J.*, *93*, 1402–1412, doi:10.1529/biophysj.107.107474.

Farina, M., D. M. S. Esquivel, and H. G. P. L. de Barros (1990), Magnetic iron-sulphur crystals from a magnetotactic microorganism, *Nature*, *343*, 256–258.

Fassbinder, J. W. E., H. Stanjek, and H. Vali (1990), Occurence of magnetic bacteria in soil, *Nature*, *343*, 161–162.

Fischer, A. (1996), Isotopengeochemische Untersuchungen ($\delta^{18}O$ und $\delta^{13}C$) im wasser und in den sedimenten des Soppensees (Kt. Luzern, Schweiz), Ph.D. thesis, Eidgenössische Tech. Hochsch., Zurich.

Fischer, A., M. Schmitz, B. Aichmayer, P. Fratzl, and D. Faivre (2011), Structural purity of magnetite nanoparticles in magnetotactic bacteria, *J. R. Soc. Interface*, *8*, 1011–1018, doi:10.1098/rsif.2010.0576.

Fischer, H., G. Mastrogiacomo, J. F. Löffler, R. J. Warthmann, P. G. Weidler, and A. U. Gehring (2008), Ferromagnetic resonance and magnetic characteristics of intact magnetosome chains in *Magnetospirillum Gryphiswaldense*, *Earth Planet. Sci. Lett.*, *270*, 200–208.

Flies, C. B., H. M. Jonkers, D. de Beer, K. Bosselmann, M. E. Böttcher, and D. Schüler (2005), Diversity and vertical distribution of magnetotactic bacteria along chemical gradients in freshwater microcosms, *FEMS Microbiol. Ecol.*, *52*, 185–195, doi:10.1016/j.femsec.2004.11.006.

Frankel, R., and R. Blakemore (1980), Magnetotaxis and bacteria, *J. Phys.*, *41*, 1–28.

Frankel, R. B., R. P. Blakemore, and R. S. Wolfe (1979), Magnetite in freshwater magnetotactic bacteria, *Science*, *203*, 1355–1356, doi:10.1126/science.203.4387.1355.

Gehring, A. U., H. Fischer, M. Louvel, K. Kunze, and P. G. Weidler (2009), High temperature stability of natural maghemite: A magnetic and spectroscopic study, *Geophys. J. Int.*, *179*, 1361–1371, doi:10.1111/j.1365-246X.2009.04348.x.

Gehring, A. U., J. Kind, M. Charilaou, and I. Garcia-Rubio (2011), The detection of magnetotactic bacteria and magnetofossils by means of magnetic anisotropy, *Earth Planet. Sci. Lett.*, doi:10.1016/j.epsl.2011.06.024, in press.

Granwehr, J., P. G. Weidler, and A. U. Gehring (2004), The fate of structure-bound Mn^{2+} during the decomposition of dolomite and in the resulting conversion products: An EPR study, *Am. Mineral.*, *89*, 785–789.

Hall, P. L., B. R. Angel, and J. Braven (1974), Electron spin resonance and related studies of lignite and ball clay from South Devon, England, *Chem. Geol.*, *13*, 97–113.

Haltia-Hovi, E., N. Nowaczyk, T. Saarinen, and B. Plessen (2010), Magnetic properties and environmental changes recorded in Lake Lehmilampi (Finland) during the Holocene, *J. Paleolimnol.*, *43*, 1–13.

Hanzlik, M., M. Winklhofer, and N. Petersen (2002), Pulsed-field-remanence measurements on individual magnetotactic bacteria, *J. Magn. Magn. Mater.*, *248*, 258–267.

Housen, B. A., and B. M. Moskowitz (2006), Depth distribution of magnetofossils in near-surface sediments from the Blake/Bahama Outer Ridge, western North Atlantic Ocean, determined by low-temperature magnetism, *J. Geophys. Res.*, *111*, G01005, doi:10.1029/2005JG000068.

Jacobs, I. S., and C. P. Bean (1955), An approach to elongated fine-particle magnets, *Phys. Rev. Lett.*, *100*, 1060–1067, doi:10.1103/PhysRev.100.1060.

Johnson, H. P., W. Lowrie, and D. V. Kent (1975), Stability of anhysteretic remanent magnetization in fine and coarse magnetite and maghemite particles, *Geophys. J. R. Astron. Soc.*, *41*, 1–10.

Kakol, Z., and J. M. Honig (1989), Influence of deviations from ideal stoichiometry on the anisotropy parameters of magnetite $Fe_{3(1-\delta)}O_4$, *Phys. Rev. B*, *40*, 9090–9097, doi:10.1103/PhysRevB.40.9090.

Kalmijn, A. (1981), Biophysics of geomagnetic field detection, *IEEE Trans. Magn.*, *17*, 1113–1124, doi:10.1109/TMAG.1981.1061156.

Kim, B., K. P. Kodama, and R. E. Moeller (2005), Bacterial magnetite produced in water column dominates lake sediment mineral magnetism: Lake Ely, USA, *Geophys. J. Int.*, *163*, 26–37, doi:10.1111/j.1365-246X.2005.02735.x.

Kirschvink, J. L. (1980), South-seeking magnetic bacteria, *J. Exp. Biol.*, *86*, 345–347.

Kirschvink, J. L. (1982), Paleomagnetic evidence for fossil biogenic magnetite in western Crete, *Earth Planet. Sci. Lett.*, *59*, 388–392.

Kobayashi, A., J. L. Kirschvink, C. Z. Nash, R. E. Kopp, D. A. Sauer, L. E. Bertani, W. F. Voorhout, and T. Taguchi (2006), Experimental observation of magnetosome chain collapse in magnetotactic bacteria: Sedimentological, paleomagnetic, and evolutionary implications, *Earth Planet. Sci. Lett.*, *245*, 538–550.

Kopp, R. E., and J. L. Kirschvink (2008), The identification and biogeochemical interpretation of fossil magnetotactic bacteria, *Earth-Sci. Rev.*, *86*, 42–61.

Kopp, R. E., C. Z. Nash, A. Kobayashi, B. P. Weiss, D. A. Bazylinski, and J. L. Kirschvink (2006), Ferromagnetic resonance spectroscopy for assessment of magnetic anisotropy and magnetostatic interactions: A case study of mutant magnetotactic bacteria, *J. Geophys. Res.*, *111*, B12S25, doi:10.1029/2006JB004529.

Lascu, I., S. K. Banerjee, and T. S. Berquó (2010), Quantifying the concentration of ferrimagnetic particles in sediments using rock magnetic methods, *Geochem. Geophys. Geosyst.*, *11*, Q08Z19, doi:10.1029/2010GC003182.

Lins, U., M. R. McCartney, M. Farina, R. B. Frankel, and P. R. Buseck (2005), Habits of magnetosome crystals in coccoid magnetotactic bacteria, *Appl. Environ. Microbiol.*, *71*, 4902–4905.

Lotter, A. (2001), The paleolimnology of Soppensee (Central Switzerland), as evidenced by diatoms, pollen, and fossil-pigment analyses, *J. Paleolimnol.*, *25*, 65–79.

Løvlie, R., and E. Larsen (1981), Paleomagnetism and magnetomineralogy of a Holocene lake sediment from Vagson, Western Norway, *Phys. Earth Planet. Inter.*, *27*, 143–150.

Lowrie, W., and M. Fuller (1971), On the alternating field demagnetization characteristics of multidomain thermoremanent magnetization in magnetite, *J. Geophys. Res.*, *76*, doi:10.1029/JB076i026p06339.

Maher, B. A., and R. M. Taylor (1988), Formation of ultrafine-grained magnetite in soils, *Nature*, *336*, 368–370.

Mann, S., N. Sparks, and R. Blakemore (1987), Ultrastructure and characterization of anisotropic magnetic inclusions in magnetotactic bacteria, *Proc. R. Soc. B*, *231*, 469–476.

Mann, S., N. H. C. Sparks, R. B. Frankel, D. A. Bazylinski, and H. W. Jannasch (1990), Biomineralization of ferrimagnetic greigite (Fe_3S_4) and iron pyrite (FeS_2) in a magnetotactic bacterium, *Nature*, *343*, 258–261.

Mastrogiacomo, G., H. Fischer, I. Garcia-Rubio, and A. Gehring (2010), Ferromagnetic resonance spectroscopic response of magnetite chains in a biological matrix, *J. Magn. Magn. Mater.*, *322*, 661–663, doi:10.1016/j.jmmm.2009.10.035.

Moskowitz, B., R. Frankel, P. Flanders, R. P. Blakemore, and B. B. Schwartz (1988), Magnetic properties of magnetotactic bacteria, *J. Magn. Magn. Mater.*, *73*, 273–288.

Moskowitz, B., R. B. Frankel, and D. Bazylinski (1993), Rock magnetic criteria for the detection of biogenic magnetite, *Earth Planet. Sci. Lett.*, *120*, 283–300.

Moskowitz, B. M., D. A. Bazylinski, R. Egli, R. B. Frankel, and K. J. Edwards (2008), Magnetic properties of marine magnetotactic bacteria in a seasonally stratified coastal pond (Salt Pond, MA, USA), *Geophys. J. Int.*, *174*, 75–92, doi:10.1111/j.1365-246X.2008.03789.x.

Muxworthy, A. R., and W. Williams (2006), Critical single-domain/multidomain grain sizes in noninteracting and interacting elongated magnetite particles: Implications for magnetosomes, *J. Geophys. Res.*, *111*, B12S12, doi:10.1029/2006JB004588.

Newell, A. J. (2005), A high-precision model of first-order reversal curve (FORC) functions for single-domain ferromagnets with uniaxial anisotropy, *Geochem. Geophys. Geosyst.*, *6*, Q05010, doi:10.1029/2004GC000877.

Oldfield, F., R. Wake, J. Boyle, R. Jones, S. Nolan, Z. Gibbs, P. Appleby, E. Fisher, and G. Wolff (2003), The late-Holocene history of Gormire Lake (NE England) and its catchment: A multiproxy reconstruction of past human impact, *Holocene*, *13*, 677–690, doi:10.1191/0959683603hl654rp.

Özdemir, O., D. J. Dunlop, and B. M. Moskowitz (1993), The effect of oxidation on the Verwey transition, *Geophys. Res. Lett.*, *20*, 1671–1674.

Paasche, Ø., and J. Larsen (2010), Changes in lake stratification and oxygen distribution inferred from two contrasting records of magnetotactic bacteria and diatoms, *J. Geophys. Res.*, *115*, G02012, doi:10.1029/2009JG001081.

Paasche, Ø., R. Løvlie, S. O. Dahl, J. Bakke, and A. Nesje (2004), Bacterial magnetite in lake sediments: late glacial to Holocene climate and sedimentary changes in northern Norway, *Earth Planet. Sci. Lett.*, *223*, 319–333.

Pan, Y., N. Petersen, A. F. Davila, L. Zhang, M. Winklhofer, Q. Liu, M. Hanzlik, and R. Zhu (2005), The detection of bacterial magnetite in recent sediments of Lake Chiemsee (Southern Germany), *Earth Planet. Sci. Lett.*, *232*, 109–123, doi:10.1016/j.epsl.2005.01.006.

Penninga, I., H. de Waard, B. M. Moskowitz, D. A. Bazylinski, and R. B. Frankel (1995), Remanence measurements on individual magnetotactic bacteria using a pulsed magnetic field, *J. Magn. Magn. Mater.*, *149*, 279–286, doi:10.1016/0304-8853(95)00078-X.

Petermann, H., and U. Bleil (1993), Detection of live magnetotactic bacteria in South Atlantic deep-sea sediments, *Earth Planet. Sci. Lett.*, *117*, 223–228, doi:10.1016/0012-821X(93)90128-V.

Petersen, N., T. von Dobeneck, and H. Vali (1986), Fossil bacterial magnetite in deep-sea sediments from the South Atlantic Ocean, *Nature*, *320*, 611–614.

Philipse, A. P., and D. Maas (2002), Magnetic colloids from magnetotactic bacteria: Chain formation and colloidal stability, *Langmuir*, *18*, 9977–9984.

Pike, C. R., A. P. Roberts, and K. L. Verosub (1999), Characterizing interactions in fine magnetic particle systems using first order reversal curves, *J. Appl. Phys.*, *85*, 6660–6667.

Polder, D., and J. Smit (1953), Resonance phenomena in ferrites, *Rev. Mod. Phys.*, *25*(1), 89–90, doi:10.1103/RevModPhys.25.89.

Pósfai, M., P. R. Buseck, D. A. Bazylinski, and R. B. Frankel (1998), Iron sulfides from magnetotactic bacteria: Structure, composition, and phase transitions, *Am. Mineral.*, *83*(11–12), 1469–1481.

Roberts, A. P., C. R. Pike, and K. L. Verosub (2000), First-order reversal curve diagrams: A new tool for characterizing the magnetic properties of natural samples, *J. Geophys. Res.*, *105*, 28,461–28,475.

Scheffel, A., M. Gruska, D. Faivre, A. Linaroudis, P. L. Graumann, J. M. Plitzko, and D. Schüler (2006), An acidic protein aligns magnetosomes along a filamentous structure in magnetotactic bacteria, *Nature*, *440*, 110–114.

Shcherbakov, V. P., M. Winklhofer, M. Hanzlik, and N. Petersen (1997), Elastic stability of chains of magnetosomes in magnetotactic bacteria, *Eur. Biophys. J.*, *26*, 319–326.

Simmons, S. L., M. Sievert, R. B. Frankel, D. A. Bazylinski, and K. J. Edwards (2004), Spatiotemporal distribution of marine magnetotactic bacteria in a seasonally stratified coastal salt pond, *Appl. Environ. Microbiol.*, *70*, 6230–6239, doi:10.1128/AEM.70.10.6230–6239.2004.

Smirnov, A. V., and J. A. Tarduno (2000), Low-temperature magnetic properties of pelagic sediments (Ocean Drilling Program Site 805C): Tracers of maghemitization and magnetic mineral reduction, *J. Geophys. Res.*, *105*, 16,457–16,471, doi:10.1029/2000JB900140.

Snowball, I., L. Zillén, and P. Sandgren (2002), Bacterial magnetite in Swedish varved lake-sediments: A potential bio-marker of environmental change, *Quat. Int.*, *88*, 13–19, doi:10.1016/S1040-6182(01)00069-6.

Snowball, I. F. (1994), Bacterial magnetite and the magnetic properties of sediments in a Swedish lake, *Earth Planet. Sci. Lett.*, *126*, 129–142, doi:10.1016/0012-821X(94)90246-1.

Sparks, N., L. Courtaux, S. Mann, and R. Board (1986), Magnetotactic bacteria are widely distributed in sediments in the U.K., *FEMS Microbiol. Lett.*, *37*, 305–308.

Stolz, J. F., S.-B. R. Chang, and J. L. Kirschvink (1989), Biogenic magnetite in stromatolites. I. Occurrence in modern sedimentary environments, *Precambrian Res.*, *43*, 295–304, doi:10.1016/0301-9268(89)90061-2.

Vali, H., O. Förster, G. Amarantidis, and N. Petersen (1987), Magnetotactic bacteria and their magnetofossils in sediments, *Earth Planet. Sci. Lett.*, *86*, 389–400.

Vastyn, E. P., J. Hanton, and A. Morrish (1962), Ferromagnetic resonance of single-domain particles, *Phys. Rev.*, *128*, 2078–2087.

Vonsovskii, S. V. (1966), *Ferromagnetic Resonance: The Phenomenon of Resonant Absorption of a High-Frequency Magnetic Field in Ferromagnetic Substances*, translated by H. S. H. Massey, Pergamon Press, Oxford, New York.

Weiss, B. P., S. S. Kim, J. L. Kirschvink, R. E. Kopp, M. Sankaran, A. Kobayashi, and A. Komeilia (2004), Ferromagnetic resonance and low-temperature magnetic tests for biogenic magnetite, *Earth Planet. Sci. Lett.*, *224*, 73–89.

Winklhofer, M., and N. Petersen (2007), Paleomagnetism and magnetic bacteria, in *Magnetoreception and Magnetosomes in Bacteria*, *Microbiol. Monogr.*, vol. 3, edited by D. Schüler, pp. 255–273, Springer, Berlin, doi:10.1007/7171_046.

Winklhofer, M., and G. T. Zimanyi (2006), Extracting the intrinsic switching field distribution in perpendicular media: A comparative analysis, *J. Appl. Phys.*, *99*, 08E710, doi:10.1063/1.2176598.

Wohlfarth, E. P. (1958), Relations between diffrent modes of acquisition of the remanent magnetization of ferromagnetic particles, *J. Appl. Phys.*, *29*, 595–561.

Xu, S., and D. J. Dunlop (1995), Towards a better understanding of the Lowrie-Fuller test, *J. Geophys. Res.*, *100*, 22,533–22,542.

Zhang, Y., L. Sun, Y. Fu, Z. Huang, X. Bai, Y. Zhai, J. Du, and H. Zhai (2009), The shape anisotropy in the magnetic field-assisted self-assembly chain-like structure of magnetite, *J. Phys. Chem.*, *113*, 8152–8157.